

## GEOLOGIC MAP OF THE SAPPHO PATERA QUADRANGLE (V-20), VENUS

By George E. McGill

### INTRODUCTION

The Sappho Patera quadrangle (V-20) of Venus is bounded by 0° and 30° East longitude, 0° and 25° North latitude. It is one of 62 quadrangles covering the entire planet at a scale of 1:5,000,000. The quadrangle derives its name from Sappho Patera, a large rimmed depression (diameter about 225 km) lying on top of a shield-shaped mountain named Irnini Mons. Sappho, a noted Greek poet born about 612 B.C., spent most of her life on the island of Lesbos. All of her works were burned in 1073 by order of ecclesiastical authorities in Rome and Constantinople. What little survives was discovered in 1897 as parts of papier mâché coffins in the Fayum (Durant, 1939).

The Sappho Patera quadrangle includes the central portion of Eistla Regio, an elongated, moderately elevated (relief ~1 km) region extending for about 7,500 km west-northwestward from the west end of Aphrodite Terra. It is generally interpreted to be the surface manifestation of one or more mantle plumes (Phillips and Malin, 1983; Stofan and Saunders, 1990; Kiefer and Hager, 1991; Senske and others, 1992; Grimm and Phillips, 1992; Solomon and others, 1992). Eistla Regio is dominated by several large volcanic features. All or parts of four of these occur within the Sappho Patera quadrangle: the eastern flank of Gula Mons, Irnini Mons, Anala Mons, and Kali Mons. The quadrangle also includes eight named coronae: Nehalennia, Sunrta, Libera, Belet-Ili, Gaia, Asomama, Rabzhima, and Changko. A major rift extends from Gula Mons in the northwestern corner of the quadrangle to Libera Corona near the east border. East of Irnini and Anala Montes this rift is named Guor Linea; west of the montes it is named Virtus Linea. In addition to these major features, the Sappho Patera quadrangle includes numerous smaller volcanic flows and constructs, several unnamed coronae and corona-like features, a complex array of faults, fractures, and wrinkle ridges, and extensive plains that are continuous with the regional plains that constitute about 80% of the surface of Venus (Masursky and others, 1980).

This area is geologically interesting because it contains examples of most globally important types of features and deposits and is an excellent area to study the temporal and genetic relations among plains, rifts, coronae, and large shield volcanoes. The temporal relations displayed in this quadrangle can provide useful constraints on models for venusian tectonic style (McGill, 1994b).

### METHODS AND DATA USED

Mapping was based on both hard-copy and digital versions of Magellan synthetic aperture radar (SAR) data, mostly from cycle 1, but much of the area also is covered by cycle 3 images. During both of these cycles the data were collected in a left-looking mode. In cycle 1, the SAR incidence angles for images taken of the Sappho Patera quadrangle ranged from 44° to 46°; in cycle 3, they ranged from 25° to 26°. SAR data include full-resolution (75 m/pxl) and compressed-once (225 m/pxl) digital images provided on compact disks by the Jet Propulsion Laboratory, and 1:1,500,000 photographic prints of 12° × 12° sub-areas at 75 m/pxl (F-MAP's) prepared by the U.S. Geological Survey. The base map is a 1:5,000,000-scale controlled mosaic of Magellan cycle 1 SAR data, also prepared by the U.S. Geological Survey. Topographic information was derived from digital elevation models and from gridded elevation data, both prepared at the Massachusetts Institute of Technology and distributed on compact disks. The altimetry data were combined with the SAR data by the U.S. Geological Survey to create synthetic stereoscopic images.

Stratigraphic material units were defined primarily by their relative radar brightness and surface textures, although crosscutting relations with structures, relative ages, and apparent association with topographic or structural features also were considered where appropriate and useful. All units were defined using cycle 1 data. Because these images were all taken with large incidence angles, the relative radar brightness of the various map units relate primarily to surface roughness at a scale comparable to the radar wavelength (12.6 cm). Characteristic values of important radar properties (radar backscatter coefficient, emissivity, reflectivity, and root mean square slope) were calculated for each material unit using programs provided by Campbell (1995). However, these properties were not used in the original unit definitions, which were based entirely on visual properties apparent in the SAR images. The primary value of the radar parameters is in facilitating correlation with possibly similar units elsewhere on Venus where the SAR incidence angles were different. These parameters also provide information about the nature (grain size, surface texture, dielectric constant) of the materials making up a map unit, and thus in some instances can contribute to determining the most likely origin of the unit.

## STRATIGRAPHY

The stratigraphic units in the Sappho Patera quadrangle are grouped into six broad categories according to topographic setting or terrain type: tessera, plains, coronae, miscellaneous flows and domes on plains, central volcanoes, and impact craters. Thirty-three units have been defined: one tessera unit, eight plains units, six flow units associated with coronae, five miscellaneous flow and dome units, eleven units associated with central volcanoes, and two impact-crater units. Most unit names are based on characteristics visible on SAR images. Those units clearly associated with a structural or topographic feature or type of feature are named so that this association is explicit. Relative ages of units were determined primarily by embayment relations and truncation of structures at contacts. Because of small numbers and globally random distribution, the density of impact craters cannot be used to determine the relative ages of map units. Quantitative radar properties for most units are summarized in table 1; a representative subset of units is also compared (fig. 1) with the average scattering of the Venus surface as described by the Muhleman law (Muhleman, 1964)

### TESSERA MATERIALS

Scattered within the Sappho Patera quadrangle are small, radar-bright inliers projecting through younger plains materials. The material constituting these inliers is comparable to that found within tessera terrain, as defined from Venera images (Basilevsky and others, 1986). All tessera material (unit *t*) has been intensely deformed into at least two sets of structures at high angles to each other. Some of these structures are grabens that are large enough for diagnostic criteria to be clearly visible on the Magellan images. The surrounding plains materials embay the tessera material, flood the large grabens, and abruptly truncate most or all other structures that crosscut the tessera material. On the basis of structural and stratigraphic evidence, tessera material is older than all other units within the quadrangle. Unequivocal and geographically widespread superposition evidence of relative age exists for all units except lineated plains and textured plains materials. Tessera material is in contact with lineated plains material at only one locality and is not in contact with textured plains material at any locality. Because tessera material is deformed by two sets of closely spaced structures, lineated plains material by only one set, and textured plains by none, the tessera material is inferred to be older than both of the others. However, some uncertainty remains because deformation events can be spatially as well as temporally limited, and thus the relative age range of tessera material is shown overlapping the ranges of lineated plains and textured plains materials on the correlation chart. Although tessera material is almost certainly older than all other materials in the quadrangle, it is not possible to determine if it represents remnants of truly ancient terrains or if it is simply highly deformed plains material that is not significantly older than the regional plains. Furthermore, it is not possible to determine if the various patches of tessera contain material of similar age; in fact, these materials could be of widely differing ages.

## PLAINS MATERIALS

Most plains materials are characterized by intermediate brightness on the SAR images; the exceptions include the oldest and the youngest plains materials. Scattered about the quadrangle are generally very small inliers of bright to extremely bright lineated plains material (unit *pl*). At one locality (17.5° N., 4.5° E.), lineated plains material embays tessera material. All inliers of lineated plains material are embayed by, and thus older than, the surrounding regional plains materials. Lineated plains material is generally characterized by one set of closely spaced linear features (probably faults or fractures) that are truncated at contacts with the surrounding plains. In the Sappho Patera quadrangle, most of these linear features trend within about 10° of north-south. The large grabens that cut most areas underlain by tessera material are less common in inliers of lineated plains material, and where they do occur, they parallel the trend of the bright linear features that define the unit. Locally, lineated plains material is not severely deformed (see, for example, table 1, unit *pl* station 1); in such places it is not as bright as where severely deformed (table 1, unit *pl* stations 2, 3), but still brighter than typical regional plains, thus suggesting that the enhanced brightness is due both to high surface roughness and to relatively steep local slopes produced by deformation. For many small bright patches on the plains it is very difficult to determine if the brightness is due to the presence of lineated plains material or to locally enhanced fracturing of the younger regional plains. Therefore, the lineated plains material simply may be older, rougher, and generally more deformed plains material that otherwise is not fundamentally different from more typical regional plains materials.

Northeast and east of Irnini Mons are three areas of textured plains material (unit *pt*) defined by irregular radar-bright lines and spots at about 1 km scale. Some of this material has been deformed into gentle ridges more than 1 km wide and up to 100 km long. Textured plains material is embayed by regional plains material member *b*; its age relative to lineated plains and tessera materials cannot be determined directly, but textured plains material is inferred to be younger because it lacks the intense fabrics that characterize these other materials.

Most of the Sappho Patera quadrangle is underlain by regional plains materials, which are mapped as three members: regional plains material members *a* (unit *pr<sub>a</sub>*), *b* (unit *pr<sub>b</sub>*), and *c* (unit *pr<sub>c</sub>*). Member *b* is by far the most widespread unit in the quadrangle. Although this unit exhibits a range of radar backscatter values, its most common signature lies very close to the planetary mean Muhleman law curve (see fig. 1, unit *pr<sub>b</sub>*, station 5). Although the three members can be separated and mapped within the regional plains in some places, it is almost certain that elsewhere member *b* includes the other two members as patches either too small to map or with such indistinct contacts that they cannot be mapped, and thus members *a* and *c* together are shown as coeval with member *b* on the correlation chart. Member *a* includes linear features that are truncated at contacts with member *b*, implying that member *a* is older than the locally adjacent member *b*. In general, the brightness of member *a* is comparable to that of the

brighter areas of member b. Member c is present as a single area that is bright on the SAR image relative to members a and b. On the basis of the absence of linear features, member c is younger than member a and thus coeval with the younger part of member b. Regional plains materials embay tessera and lineated plains materials and are in turn

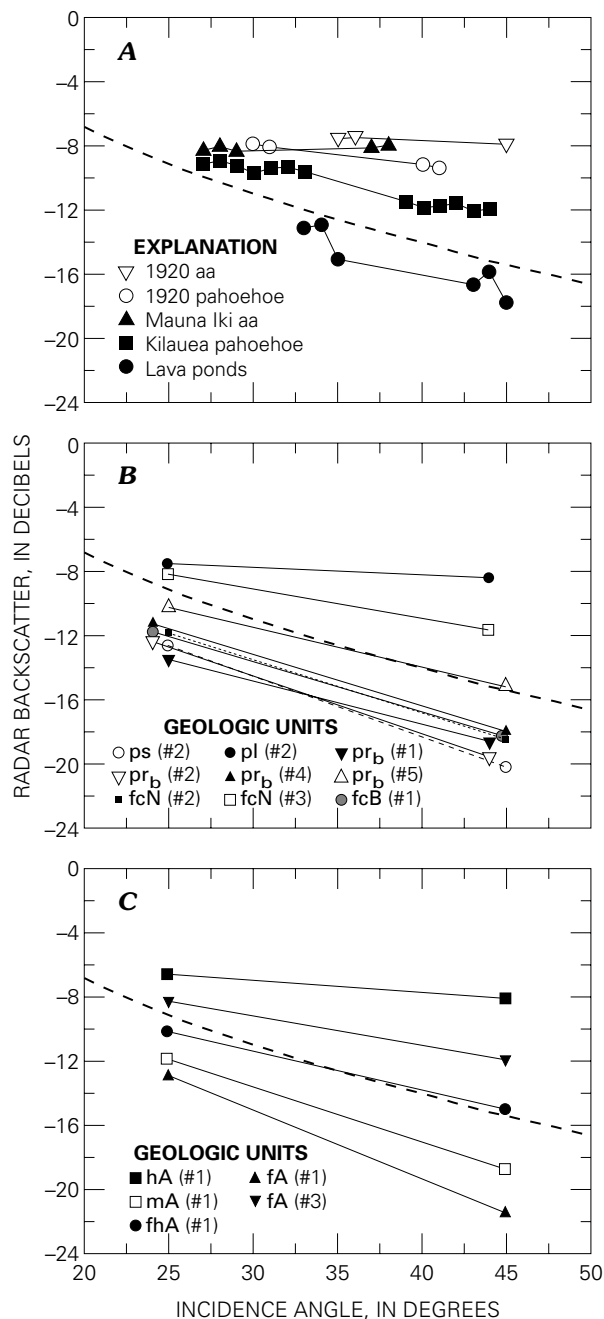


**Figure 1.** Radar backscatter properties (see table 1) of selected map units. A, Hawaiian basaltic lava (Campbell, 1995). B, Major plains and coroneae units. C, Volcanic units on Anala Mons. Units not plotted are either similar to those shown, not covered by cycle 3, or of only limited areal importance. Dashed curve represents average Venus backscatter according to Muhleman law (Muhleman, 1964).

embayed by flows derived from the four major volcanic centers Gula, Irnini, Anala, and Kali. Scattered small volcanic edifices are very common on regional plains materials, especially in the southern and north-central parts of the quadrangle. Wrinkle ridges are nearly ubiquitous but of widely varying abundance and brightness on SAR images.

Completely enclosed within regional plains material member b are four areas mapped as low-relief shield plains material (unit ps). These areas appear superficially similar to the brighter areas included in regional plains material member b. However, the areas underlain by low-relief shield plains are low rises with a relief of a few hundred meters. These rises are characterized by digitate and lobate flow lobes, and three of the four, including Dröl-ma Tholus, also have clearly visible source calderas. Low-relief shield plains material is superposed on regional plains material member b, but it formed prior to the development of all sets of wrinkle ridges present on the regional plains.

East of Irnini Mons and in the northeast corner of the quadrangle are areas with a bland, homogeneous texture and uniform, intermediate radar brightness. These areas are mapped as homogeneous plains material (unit ph). The contacts of homogeneous plains material are locally wispy, suggesting some modification by wind action. Homogeneous plains material truncates structures within textured plains material. Its age relative to regional plains materials is less clear, but locally the contacts of homogeneous plains appear affected by wrinkle ridges on regional plains, implying that the homogeneous plains material is younger.

The youngest plains unit, smooth plains material (unit ps), is present only locally as small patches. This material is clearly among the youngest in the area, because it is superposed on almost all structures and on some of the youngest lava flows derived from Irnini and Anala Montes. The radar properties of this material (table 1) indicate that its darkness is due to a very smooth surface.

### CORONA MATERIALS

Mappable flow units are associated with six coroneae: Nehalennia, Sunrta, Belet-Ili, Gaia, and two unnamed coroneae, designated a and b for mapping purposes (fig. 2<sup>1</sup>). All six flow units are named corona flow material, with an added letter designating the source corona (units fcN, fcS, fcB, fcG, fca, and fcb). These materials are generally characterized by digitate and lobate flow morphologies, which range from clearly defined to very subtle on the SAR images. Some corona flow material from Nehalennia is embayed by regional plains material member b, and some is superposed on it; thus, the deposition of this unit appears to overlap that of at least some regional plains. Corona flow materials from the other five coroneae are superposed on regional plains material member b. Corona flow materials from Belet-Ili and coroneae a and b have few or no superposed wrinkle ridges. These relations suggest that flow material from Nehalennia is the oldest, flow materials from Sunrta and Gaia are of intermediate age, and flow materials from Belet-Ili and coroneae a and b are the youngest.

<sup>1</sup> Figures 2, 3, and 4 are on map sheet.

## MISCELLANEOUS DOME AND FLOW MATERIALS

The steep-sided domes in Oshun and Carmenta Farra are large enough to map separately as Oshun Farra material (unit **dO**) and Carmenta Farra material (unit **dC**). These units are inferred to be volcanic in origin, but the eruptive mechanism and the lava composition are enigmatic. Both units are spatially associated with coronae. Carmenta Farra are adjacent to Nehalennia Corona and are cut by concentric structures related to that corona. Similarly, Oshun Farra are adjacent to Gaia Corona and are cut by structures that are concentric to Gaia Corona or radial to Belet-Ili Corona, which also is nearby.

Well-defined digitate and lobate flows are present in many places on the plains. Some flow fields are associated with concentrations of small volcanic edifices ("shield fields"), and these are mapped separately as shield-field flow material (unit **fs**). Other flows have no obvious source and are simply mapped as undifferentiated flow material (unit **f**), except for one small bright flow (2.5° N., 27° E.) with a hummocky texture (unit **fh**). All of these flow materials are superposed on regional plains material member **b**, and most have east-west wrinkle ridges superposed on them.

## MATERIALS OF CENTRAL VOLCANOES

Deposits associated with each of the four central volcanoes partly or entirely within the Sappho Patera quadrangle have been assigned names that identify the source volcano and also provide descriptive information. Clearly defined digitate flank flows of generally similar appearance are present on all four: Gula flow material (unit **fG**), Irnini flow material (unit **fl**), Anala flow material (unit **fA**), and distal (**fdK**) and proximal (**fpK**) flow materials from Kali. In addition, both Irnini and Anala Montes have mottled materials with associated abundant small shields at their summits (units **mI**, **mA**), and both have high to very high backscatter materials forming halos around their summits (units **hI**, **hA**). These halo materials have very uniform textures at F-MAP scale. Transitional units (**fhI**, **fhA**) between halo and flow materials also are present; these materials are almost as bright as the halo materials, but faint flow forms are visible as well. Radar properties (table 1) of the halo and haloed flow materials indicate that the extreme brightness must be due to significant centimeter-scale roughness. The location of these materials around the summits suggests that they could be pyroclastics; if so, they must be very coarse grained to account for the roughness. The possibility that the material forming the halos is pyroclastic is of some interest because theoretical considerations suggest that the high atmospheric pressure of Venus should inhibit exsolution of volatiles near the surface (Head and Wilson, 1986). However, other deposits of suspected pyroclastic origin have been identified at low-elevation sites even less favorable than the summits of Anala and Irnini Montes (Guest and others, 1992). The small patch of apparently similar material to the west of Irnini Mons remains enigmatic.

Flows from all four volcanoes are superposed on regional plains material member **b** and truncate wrinkle ridges present on that unit. Flows from Irnini and Anala embay Nehalennia corona flow material, and flows from

Anala embay Sunrta corona flow material. Flows from Anala also truncate concentric structures of Nehalennia, Sunrta, and an unnamed corona east of Nehalennia. Irnini and Anala halo materials are superposed on proximal Irnini and Anala flow materials. Irnini and Anala mottled materials appear to embay the haloed materials, and thus also must be younger than at least the proximal parts of Irnini and Anala flow materials. Flows from Anala are superposed on flows from Irnini. The presence of a few wrinkle ridges superposed on Kali distal flow material and the offset of some Gula flow material by faults associated with Guor Linea suggest that these materials are the oldest of the exposed materials related to the central volcanoes.

## IMPACT CRATER MATERIALS

Deposits of 18 impact craters occur in the quadrangle, including Afiruwa, Agoe, Akuba, Aminata, Annia Faustina, Callas, Devorguilla, Esther, Faufau, Festa, Hiriata, Kelea, Manton, Margarita, Piaf, a portion of Mona Lisa, and 2 small craters without names. In addition, there are two "splotch" features, one too small to map (24.1° N., 0.4° E.), the other centered at 24.8° N., 22.7° E. These apparently are deposits of fragmental material from bolides that did not reach the surface (Campbell and others, 1992). Two impact-crater units are mapped: undifferentiated material of central peaks, floors, rims, and ejecta (unit **c**), and material of fluid flow deposits (unit **cf**). Most of these materials are radar-bright due to rough surfaces. Crater floor material is radar-bright in some craters, radar-dark in others. The bright floors are inferred to be rough fall-back deposits, whereas the dark floors are most likely relatively smooth, ponded impact melt (Grieve and Cintala, 1995). Several of the craters produced digitate flow features, and two small impact structures appear to have produced abundant flow material but little or no ejecta. Annia Faustina, an unnamed crater centered at 3° N., 5° E., and one or more craters in the cluster including Festa, Manton, and Kelea have associated radar-dark parabolic halos. Two of these halos also are characterized by emissivity that is lower than the surrounding surface, but the Annia Faustina halo has an emissivity that is higher than the surrounding surface (fig. 3).

All of the craters and splotches are younger than regional plains materials. Three craters (Annia Faustina, Kelea, and Manton) and the smaller splotch are demonstrably younger than flows from young central volcanoes, one crater (Festa) appears to be older than the distal flows from Kali, and the rest are not in contact with deposits of central volcanoes and thus are of unknown age relative to the flows from these volcanoes.

## SURFICIAL MATERIALS

Indications of probable aeolian activity affecting surface properties include the wispy nature of some of the contacts of the homogeneous plains material (unit **ph**), mentioned above. This effect appears to be minor and thus not likely to have affected placement of the unit contact significantly. Other surficial deposits are the impact-related splotches and halos discussed under impact crater materials above. The larger splotch is shown by a stipple pattern on the geologic

map. The crater halos are not shown on the map but can be identified in the emissivity data (fig. 3).

## STRUCTURAL GEOLOGY

Structures inferred to be fractures, faults, or folds are extremely abundant and of widely diverse scales, ranging in size from linear features a few kilometers long to complex fault and fracture zones more than a thousand kilometers long. In this section of the text, the important structures and structural types will be described; interrelationships with other features will be addressed in the following discussion section.

### MAJOR STRUCTURAL FEATURES

The largest structural feature in the map area is the Guor Linea rift, originally defined to extend along the Eistla Regio rise from Idem-Kuva Corona, north-northwest of Gula Mons (west of the map area), to the vicinity of Nehalennia Corona, west of Irnini and Anala Montes (Solomon and others, 1991, 1992; Senske and others, 1992). A similar structure, now named Virtus Linea, that is approximately aligned with Guor Linea as originally defined appears at the eastern limit of Irnini and Anala flows and continues eastward to Libera Corona, in the east-central part of the Sappho Patera quadrangle. The bounding faults of Guor and Virtus Lineae clearly cut lineated plains material (unit pl) and regional plains material member b (unit pr<sub>b</sub>). These faults are not present on Irnini and Anala Montes and are sharply truncated by the contact at the eastern limit of lava from these volcanoes. These relations suggest that Guor and Virtus Lineae were once continuous but have been completely buried by lava from Irnini and Anala Montes. The original length of the rift was thus about 2,000 km (fig. 2). The bounding faults of Guor Linea exhibit a complex, en echelon pattern, with displacement stepping from one segment to the next on linking relay faults. Because the rift trend is approximately parallel to the look direction of the Magellan SAR, the small-scale morphologic details of some of the largest fault scarps bounding it are clearly imaged. The scarps are irregular parallel to strike and exhibit ribs and flutes oriented approximately down-dip. At its widest point, the rift is about 100 km across, but a width of 50 km is more typical. Depths range up to a kilometer or more (see fig. 4 on map sheet). The rift records a complex fracture history (Grimm and Phillips, 1992) with more than one generation of faults. Several coronae are spatially associated with Guor and Virtus Lineae. These include Idem-Kuva, Nehalennia, Libera, small coronae a and b, and a small corona east of Nehalennia.

A second deformation zone, Badb Linea, extends in a broad, concave-westward arc from north of Irnini Mons southward to Sunrta Corona (fig. 2). The zone consists of long, closely spaced bright linear features, many of which can be resolved as grabens. Most of these structures are truncated by lava from Irnini Mons, but others continue on and crosscut all of the formations associated with both Irnini and Anala Montes. Thus, unlike Guor and Virtus Lineae, which must be entirely older than at least the youngest lava

from the montes, Badb Linea was active both before and after the young lavas. No evidence exists from small-scale structures for any zone-parallel shear; however, the minor misalignment of Guor and Virtus Lineae west and east of Irnini and Anala Montes could be explained by a component of sinistral strike-slip offset in addition to the more obvious extension implied by the grabens.

South of Guor Linea is a linear topographic trough extending from about the western boundary of the quadrangle eastward almost to the limit of lava flows from Anala Mons (figs. 3, 4). This feature consists of a chain of ovoidal depressions with radar-bright, topographically raised rims; the easternmost of these depressions is Changko Corona. Abundant wrinkle ridges occur within and parallel to the trough.

### RADAR-BRIGHT LINEAR FEATURES

As is commonly the case over much of Venus, the Sappho Patera quadrangle includes a perplexing array of straight to arcuate radar-bright linear features. Most of these are too narrow to determine their geometries, but in places members of linear sets are wide enough, or a single linear feature is locally wide enough, to resolve graben geometry. Thus, most straight and arcuate, radar-bright linear features are inferred to be small faults or fractures of extensional origin. Individual linear features range in length from the limit of detection (1 or 2 km in length) to hundreds of kilometers. Some occur as sets radial or concentric to coronae; Belet-Ili shows particularly good examples of radial linear features, whereas Nehalennia and Sunrta provide good examples of concentric linear features. Other sets of long, parallel linear features are associated with elevated regions of low relief and unknown origin; examples may be seen around 8° N., 2° E. and 1° N., 11° E. Much shorter examples (a few to tens of kilometers long) commonly occur as en echelon arrays or even as dense fabrics that approach being penetrative at the scale of the radar images. To varying degrees, all of the plains areas contain these small linear features, although their abundance varies widely. A particularly interesting occurrence is on the plains north of Irnini Mons, where two sets of short linear fractures occur, one trending north-northeast, the other north-northwest. Fractures of both of these sets have influenced the later development of the large grabens of Badb Linea; the grabens locally formed as a series of en echelon segments parallel to one or the other of these arrays even though the overall trend of the grabens is oblique to both of them. The most prominent example of a nearly penetrative fabric of linear features occurs at 15.5° N., 13.5° E. Although these small-scale linear features probably are of extensional origin, their structural significance remains to be deciphered.

### WRINKLE RIDGES

Sinuuous, radar-bright linear features, generally inferred to be wrinkle ridges, are present on most plains and older flow materials. These range in length from a few kilometers to hundreds of kilometers and have widths generally less than one kilometer. Wrinkle ridges are extremely abundant on the plains materials of the Sappho Patera quad-

range, as is true for most of the plains of Venus (Solomon and others, 1992; Squyres and others, 1992b; Bilotti and others, 1993). A variety of structural and volcanic hypotheses have been proposed to explain wrinkle ridges on the Moon and Mars, as reviewed by Maxwell and others (1975) and Plescia and Golombek (1986). All current genetic models explain wrinkle ridges as due to some combination of thrust faulting and folding in response to compression normal to the ridge trends, except where these trends follow older structures (McGill, 1993). Because of their abundance, wrinkle ridges on Venus can provide regional to global clues concerning stress orientations in the shallow crust and may also serve as at least local stratigraphic timelines (Bilotti and others, 1993; McGill, 1993).

The Sappho Patera quadrangle includes two sets of wrinkle ridges of regional significance (fig. 2). The dominant set defines a wavy pattern trending east-west  $\pm 20^\circ$ . This set is present over a much larger area than this quadrangle (McGill, 1993). This set also is the oldest, based on relations at "T" intersections with wrinkle ridges of other sets: wrinkle ridges of the east-west set form the cross-bar of the "T", and thus are older. The second, younger set of wrinkle ridges forms a ring almost entirely around the topographic high formed by Irnini and Anala Montes (fig. 2). These two sets record a change in orientation of shallow crustal stresses from compression north-south to compression radial to the two large montes. A similar relation exists in the vicinity of Sif and Gula Montes in western Eistla Regio (Basilevsky, 1994; McGill, 1994b). In addition to these two regionally important sets of wrinkle ridges, more local wrinkle ridges occur as a north-south set near the northwest corner, a west-convex set along the eastern boundary, a north-south set in the southeast corner of the quadrangle, and sets related to some coronae and chains of corona-like features.

Almost all wrinkle ridges are younger than regional plains, the only exception being the small east-west wrinkle ridges on Nehalennia flow material that are truncated along the contact with regional plains member *b*. Flows from the four major volcanic centers are superposed on wrinkle ridges of all sets in contact with these flows. Of the 18 impact craters that are entirely or partially within the quadrangle, 13 are demonstrably younger than the oldest, east-west-trending set of wrinkle ridges; the remaining 5 have ambiguous ages relative to old wrinkle ridges. Two craters appear to be older, and nine younger, than one or more of the younger sets of wrinkle ridges, leaving seven craters with ambiguous ages relative to younger wrinkle ridges.

#### RIDGE BELTS

The Sappho Patera quadrangle does not contain extensive, well developed ridge belts of the type common in the Vinmara Planitia area of the northern hemisphere and in the Lavinia Planitia area of the southern hemisphere (Sukhanov and others, 1989; Frank and Head, 1990; Squyres and others, 1992b; Solomon and others, 1992; Ivanov and Head, in press; Rosenberg and McGill, in press). However, textured plains material (unit *pt*) is characterized by a few relatively small, arcuate ridges up to 100 km long and 5

km wide. These ridges contrast with wrinkle ridges, which are sinuous in plan and much narrower. The textured plains unit, and its associated ridges, is confined to a small area east and northeast of Irnini Mons. It possibly represents the remnant of a once more extensive ridge belt now buried by regional plains and Irnini lava, but insufficient evidence exists to prove or disprove this conjecture.

#### VOLCANIC FEATURES

The area is dominated by all or parts of four volcanic edifices: Gula, Irnini, Anala, and Kali Montes. All four have the gentle flank slopes and overall shapes characteristic of shield volcanoes. Gula Mons is characterized by slope angles between  $0.25^\circ$  and  $1.4^\circ$  (Senske and others, 1992). Irnini Mons is about 475 km wide and 1.75 km high. Sappho Patera in its summit region is a rimmed depression about 225 km wide and several hundred meters deep. Anala Mons is about 550 km wide and 2.25 km high. Kali Mons is about 350 km wide and 2.5 km high. Thus, average flank slopes for Irnini and Anala Montes are about  $0.5^\circ$ , for Kali Mons about  $0.8^\circ$ . Lavas from all of the edifices extend well beyond the topographic break in slope that has been used to estimate edifice diameters. Individual flows attain lengths as great as 200–250 km. Both the shield shape and the great lengths of individual flows point to a relatively low viscosity, presumably basaltic, magma composition.

The summit regions of Irnini and Anala Montes are deformed by fracture and graben complexes dominated by structures parallel to Badb Linea, but which also include radial structures on both edifices, and concentric structures on Irnini as well. Indeed, the summit structures of both Irnini and Anala Montes are listed as coronae or corona-like features by Stofan and others (1992). The large rimmed depression, Sappho Patera, at the summit of Irnini Mons is particularly interesting because it has many characteristics of a corona. McGovern (1996) interprets the composite nature of Irnini Mons as indicating formation at a time when the thickness of the lithosphere approximated the critical value separating thin lithosphere that favors corona development from thick lithosphere that favors shield volcano development. In contrast to Irnini and Anala, the summit region of Kali Mons includes only limited radial fractures and crater chains of the type commonly found on shield volcanoes.

Of particular interest are the several domes with steep sides and flat tops. These are examples of the enigmatic steep-sided domes that occur in many places on Venus (Pavri and others, 1992). Within this quadrangle are two of the largest of these, with diameters of 61 and 63 km and heights on the order of 500–800 m (Carmenta Farra). Also present is an interesting cluster of coalesced steep-sided domes (Oshun Farra), one of which appears to have lost material from part of its periphery by mass wasting. Several smaller steep-sided domes also are present. All of these features in the Sappho Patera quadrangle appear to be spatially associated with coronae; whether this also implies a genetic connection is not clear at present. The domes of Carmenta Farra are cut by fractures concentric to

Nehalennia Corona (Bridges and McGill, 1996) but have an ambiguous age relation with Nehalennia flow material. Likewise, the domes of Oshun Farra are cut by fractures associated with Belet-Ili and Gaia Coronae (Bridges and McGill, 1996). East-west wrinkle ridges apparently are diverted around the easternmost dome of Oshun Farra, indicating that the dome is older, but the evidence supporting this is not definitive.

Small volcanic edifices of various shapes are extremely abundant. These range in size from the limit of resolution to about 10 km in diameter, but there is no natural break between these and the much less abundant features of larger size. Many of these small edifices occur in clusters that can include scores to hundreds of individuals; these are the "shield fields" of Aubele and others (1992). Small edifices are relatively abundant on the plains in the southern part of the quadrangle, and apparently account for at least part of the large-scale mottled appearance of the plains in that area. They are less abundant in the northern part of the quadrangle, but a large shield field occurs north of Irnini Mons, in association with the northern end of Badb Linea. Smaller shield fields occur in association with mottled materials (units mI and mA) in the summit regions of Irnini and Anala Montes, and in the interiors of the coronae Belet-Ili, Gaia, and b. In addition to these notable concentrations of small shields and domes, scattered individuals occur widely on the plains.

Other volcanic features include flows superposed on plains materials, Nepra Vallis and other, unnamed lava channels, and scattered sub-circular pits. Most of the flows are associated with shield fields or coronae, but a few, including Merisa Fluctus, seem not to be related to any identifiable source. Many of the pits occur in association with shields or domes, but others are simply isolated individuals.

## CORONAE

The several coronae included within this quadrangle exhibit much of the structural and topographic variety characteristic of these interesting features (Stofan and others, 1992; Squyres and others, 1992a). Sunrta is essentially a large depression with a moderately elevated rim and intensely developed concentric structures. Gaia has a complex internal topography, partly higher and partly lower than the surrounding plains, and a moat that bounds the interior for at least half the circumference of the structure. Neither concentric nor radial structures are strongly developed. Libera, Belet-Ili, and Nehalennia all have complex internal topography similar to that of Gaia, but apparently no moats. Concentric structures are prominent for Nehalennia, more modest for Belet-Ili and Libera; all three have associated radial structures, and these are especially well developed and areally extensive around Belet-Ili. The unnamed coronae are generally delineated by concentric structures, but they are too small to separate any topographic signatures from larger surrounding features. Although a significant number of these coronae appear to be associated with Guor, Virtus, or Badb Linea, others, including two of the largest (Gaia and Belet-Ili), are not obviously associated with any other structural features.

## DISCUSSION

Although the volcanic and structural history of Eistla Regio is very complex, and certainly not entirely understood, stratigraphic and structural relations within the Sappho Patera quadrangle provide valuable data concerning the sequence of important events in the history of the region. Key observations will be discussed in this section; the resulting inferred chronology of events will be presented in the summary section.

East-west wrinkle ridges constitute the dominant set for a domain that is much larger than the Sappho Patera quadrangle (McGill, 1993), encompassing most of the plains bounding Eistla Regio. Within this domain, there apparently are no impact craters older than east-west wrinkle ridges, a relation that has been checked in detail in a block of eight quadrangles, including this one (McGill, 1994a). The relative ages of craters and wrinkle ridges are ambiguous in many instances, but for the hundred or so craters surveyed, there are no instances in which a crater was definitely older than east-west wrinkle ridges (there were instances, however, of craters older than wrinkle ridges belonging to younger sets). This implies that the time interval during which east-west wrinkle ridges were formed must have been short.

Thus, the east-west wrinkle-ridge set provides a rough time marker that is believed valid throughout Eistla Regio and adjacent plains. It is premature, however, to assume that wrinkle ridges in general can be used as global time markers (Bilotti and others, 1993; Basilevsky and Head, 1995), because it is clear even within this quadrangle that there are distinct sets of these structures and that these sets have different ages. Within the Sappho Patera quadrangle, the dominant east-west wrinkle ridges are superposed on all members of the regional plains and on homogeneous plains, and these units together cover most of the area. They are absent on smooth plains and on the youngest lavas from the four major volcanic edifices.

Concentric and radial structures related to coronae in the Sappho Patera quadrangle generally cut regional plains materials. Where east-west wrinkle ridges intersect the concentric and radial structures of some coronae, their trends are diverted, indicating that the corona-related structures are older. This relation implies that the surviving corona structures began to form after deposition of regional plains materials but prior to the development of the dominant set of wrinkle ridges. But this set of wrinkle ridges is older than all or almost all impact craters, as discussed above. The implication is that the emplacement of most plains materials and at least the initiation of corona development occurred in a geologically short period of time.

The corona story is more complex than this, however. The extensive flows north of Nehalennia are older than adjacent regional plains member **b**, as indicated by truncation relations along their common contact at 17° N., 7°–12° E. If these flows are correctly interpreted as derived from Nehalennia, then some corona flows are older than the most widespread member of the regional plains. Elsewhere, coronae flow materials appear to be superposed on regional plains, but the variable density of superposed wrinkle ridges implies a protracted development.

The younger of the two major sets of wrinkle ridges forms a pattern concentric to the large topographic high formed by Irnini and Anala Montes. The youngest lavas derived from the montes are completely devoid of wrinkle ridges, indicating that they were emplaced after both sets of wrinkle ridges were formed. However, the concentric wrinkle-ridge pattern implies that the montes existed as a topographic feature during the formation of these wrinkle ridges. A similar relation exists for Sif and Gula Montes (Basilevsky, 1994; McGill, 1994b) and has been interpreted as evidence for an early uplift phase in the development of these volcanic edifices (Basilevsky, 1994). Although this inferred early uplift phase in western Eistla Regio is consistent with evidence for early uplift in central Eistla Regio (discussed below), the characteristic shield shape of the montes and the presence of voluminous flows derived from them imply that at least some of their topography is constructional. The wrinkle-ridge data are consistent with either an uplift or a constructional early history for the montes, because the presence of the concentric wrinkle-ridge set, although implying the presence of a rise, does not constrain its genesis. There does not seem to be a concentric set of wrinkle ridges on the plains around Kali Mons, and thus there is no evidence for any early topography at this location.

The relative ages of lavas from the large montes, wrinkle ridges, and coronae structures and flows lead to the conclusion that the large volcanic edifices are younger than the coronae. This relation is verified by the superposition of Anala and Irnini Montes lavas on coronae structures and flows. Both coronae and shield volcanoes are believed to have formed over thermal plumes in the mantle (Grimm and Phillips, 1992; Senske and others, 1992; Squyres and others, 1992a; Stofan and others, 1992). Models for corona formation indicate that a thin lithosphere is required (Janes and others, 1992; Janes and Squyres, 1993), whereas recent Magellan gravity data suggest that the large shield volcanoes were formed on a thick lithosphere (Solomon and others, 1994). Thus, the geology of this area is consistent with secular cooling and thickening of the lithosphere. The tectonic implications of these relations are discussed in some detail in McGill (1994b).

Eistla Regio is a broad, gentle rise punctuated by several higher regions that are at least partly of constructional volcanic origin. The rise is presumably a result of uplift over one or more large plumes (Phillips and Malin, 1983; Stofan and Saunders, 1990; Kiefer and Hager, 1991; Grimm and Phillips, 1992). Because the most widespread member of the regional plains (unit *pr<sub>1</sub>*) is continuous over this rise, much of the relief due to internally driven uplift must be younger than most plains materials. However, the area west of Irnini Mons that is underlain by flows from Nehalennia Corona most likely began to rise before deposition of regional plains material member *b*. Nehalennia flow material is characterized by more abundant, small east-west wrinkle ridges than is the adjacent regional plains material to the north, and some of these wrinkle ridges are truncated along their common contact, as discussed above. This offlap relation implies that the younger formation pinches out southward against the contact with the older formation, suggesting that the present rise topography was already

partly in existence during deposition of the regional plains material. The offlap relation disappears gradually and the contact between Nehalennia flow material and regional plains material becomes more and more ambiguous to the west, suggesting that the early phase of uplift was confined to the area immediately west of Irnini Mons. Indeed, regional plains material member *b* is continuous across the Eistla rise west of about 6° E.

The existence of topography older than the large volcanic constructs is also suggested by other relations. Flows from Irnini Mons are clearly responding to older topography. On the west, a flow was confined by a preexisting valley (16° N., 11°–13° E.). On the east, flows are locally confined to radially oriented valleys between gentle ridges underlain by homogeneous and textured plains materials. A north-trending ridge east of Irnini Mons also constrains the lateral extent of Irnini flows and appears to have diverted some of them from an easterly to a southerly course. South-southeast of the summit of Anala Mons, and well up on the flank of the volcano, is a patch of lineated plains material. This is one of the oldest material units in the area, and thus its presence on the flank of the volcano indicates the existence of a pre-eruption rise that is close to but not coincident with the topography due to the volcano itself.

## SUMMARY

The well-recorded history of this region begins with the emplacement of the areally extensive regional plains materials. Remnants of older materials exist in the form of inliers of radar-bright, generally intensely deformed materials. These are mapped as two types: tessera material, with at least two well developed sets of deformation features trending at high angles to each other, and lineated plains material, generally deformed by one set of features. The absence of the second set of deformation features within lineated plains material suggests that it was not present when this set was imposed on tessera material, implying that the tessera and lineated plains materials are not the same age and that two episodes of deformation are required to form the observed structures. The original nature of both of these materials is unknown. It also is not possible to infer how much older these materials are than the widespread regional plains materials that surround them.

The relative age evidence provided by impact craters and wrinkle ridges indicates that most plains materials were emplaced very rapidly. If this is true globally (Strom and others, 1994), then the plains possibly formed in less than a million years. The thermal implications of such a rapid resurfacing would include a thin lithosphere. The formation of coronae in this area seems to have overlapped with the emplacement of regional plains, a time when the lithosphere was probably very thin.

The major rifts Guor and Virtus Lineae are younger than the regional plains materials. Structural interactions between rift faults and the concentric and radial structures of coronae suggest that the coronae structures are older (McGill, 1994b). On the other hand, Guor Linea cannot be followed across the center of Nehalennia Corona, which could be interpreted to imply that the corona is younger. Both are probably true, because coronae did not form in an

instant of time, and rift faulting probably also was progressive. It is clear, however, that the rift is older than at least the youngest lavas from Irnini and Anala Montes. Badb Linea, extending from the northern plains southward across Irnini and Anala Montes to Sunrta Corona, was obviously active both before and after the emplacement of the youngest lavas. Irnini and Anala Montes may be where they are because they formed where the active Badb Linea crossed the older rift.

The elongated rise of Eistla Regio began to form prior to the deposition of the youngest regional plains material, but most uplift probably occurred after the emplacement of all members of the regional plains. The greatest relief along the Eistla rise coincides with major volcanic centers, and at least part of this relief is constructional. The topography of Eistla Regio is thus due to a combination of progressive uplift and volcanic construction.

The youngest lava from Anala Mons is younger than lava from Irnini Mons. This is apparent from relations along their mutual contact, where Irnini lava is truncated, and also from the diversion of Anala lava flows by the preexisting topography of Irnini Mons (McGill, 1994b). The age of the lava from Kali Mons relative to lavas from Irnini and Anala is not known. However, the presence of a few wrinkle ridges superposed on the distal Kali lava suggests that it is older than Anala and Irnini lavas. At least some lava from Gula Mons is probably older than lavas from Irnini and Anala because they appear to be cut by fractures related to Guor Linea.

Smooth plains material is the youngest in the area. Its very smooth surface could be due to deposits of fine-grained materials by aeolian or volcanic processes or to ponding of low-viscosity lava; in either case, the surface must have escaped any deformation or other modification that could roughen it. The youngest lava from Anala Mons is locally cut by grabens and linear fractures, especially in the summit region and along the trace of Badb Linea. Otherwise, there seems to have been little activity in the region since the emplacement of the young lavas from the large volcanic edifices.

In summary, the geologic history of the Sappho Patera quadrangle records at least two old episodes of deformation, evidence of which survives only in isolated small inliers. Most of the materials in the area were apparently formed and deformed a few hundred million years ago (Strom and others, 1994) in a geologically brief interval of time. Since then, extensional deformation has occurred, much of it concentrated along major deformation zones. Associated with these deformation zones, and continuing after displacement ceased on one of them, was extensive volcanism that formed large edifices. This history appears to be much more sharply punctuated than is typical for Earth, and thus inferences concerning heat loss, rates of magma emplacement, and tectonic style based on present venusian conditions are likely to be misleading (Turcotte, 1995).

## REFERENCES CITED

- Aubele, J.C., Head, J.W., Crumpler, L.S., Guest, J.E., and Saunders, R.S., 1992, Fields of small volcanoes on Venus (shield fields)—Characteristics and implications, in Abstracts of papers submitted to the Twenty-third Lunar and Planetary Science Conference, part 1, Houston, March 16–20, 1992: Houston, Lunar and Planetary Institute, p. 47–48.
- Basilevsky, A.T., 1994, Concentric wrinkle ridge pattern around Sif and Gula, in Abstracts of papers submitted to the Twenty-fifth Lunar and Planetary Science Conference, part 1, Houston, March 14–18, 1994: Houston, Lunar and Planetary Institute, p. 63–64.
- Basilevsky, A.T., and Head, J.W., III, 1995, Global stratigraphy of Venus—Analysis of a random sample of thirty-six test areas: *Earth, Moon and Planets*, v. 66, p. 285–336.
- Basilevsky, A.T., Pronin, A.A., Ronca, L.B., Kryuchkov, V.P., Sukhanov, A.L., and Markov, M.S., 1986, Styles of tectonic deformations on Venus—Analysis of Venera 15 and 16 data, in Lunar and Planetary Science Conference, 16th, Houston, March 11–15, 1985, Proceedings, part 2: *Journal of Geophysical Research*, v. 91, supplement, p. D399–D411.
- Bilotti, F., Connors, C., and Suppe, J., 1993, Global organization of tectonic deformation on Venus, in Abstracts of papers submitted to the Twenty-fourth Lunar and Planetary Science Conference, part 1, Houston, March 15–19, 1993: Houston, Lunar and Planetary Institute, p. 107–108.
- Bridges, N.T., and McGill, G.E., 1996, Formation and modification ages of some steep-sided domes on Venus, in Abstracts of papers submitted to the Twenty-seventh Lunar and Planetary Science Conference, part 1, Houston, March 18–22, 1996: Houston, Lunar and Planetary Institute, p. 165–166.
- Campbell, B.A., 1995, Use and presentation of Magellan quantitative data in Venus mapping: U.S. Geological Survey Open-File Report 95–519, 32 p.
- Campbell, D.B., Stacy, N.J.S., Newman, W.I., Arvidson, R.E., Jones, E.M., Musser, G.S., Roper, A.Y., and Schaller, C., 1992, Magellan observations of extended impact crater related features on the surface of Venus: *Journal of Geophysical Research*, v. 97, p. 16,249–16,277.
- Durant, W., 1939, *The life of Greece*: New York, Simon and Schuster, 754 p.
- Frank, S.L., and Head, J.W., 1990, Ridge belts on Venus—Morphology and origin: *Earth, Moon and Planets*, v. 50/51, p. 421–470.
- Grieve, R.A.F., and Cintala, M.J., 1995, Impact melting on Venus—Some considerations for the nature of the cratering record: *Icarus*, v. 114, p. 68–79.
- Grimm, R.E., and Phillips, R.J., 1992, Anatomy of a venusian hotspot—Geology, gravity and mantle dynamics of Eistla Regio: *Journal of Geophysical Research*, v. 97, p. 16,035–16,054.
- Guest, J.E., Bulmer, M.H., Aubele, J., Beratan, K., Greeley, R., Head, J.W., Michaels, G., Weitz, C., and Wiles, C., 1992, Small volcanic edifices and volcanism in the plains of Venus: *Journal of Geophysical Research*, v. 97, p. 15,949–15,966.
- Head, J.W., Jr., and Wilson, L., 1986, Volcanic processes and landforms on Venus—Theory, predictions, and

- observations: *Journal of Geophysical Research*, v. 91, p. 9407–9446.
- Ivanov, M.A., and Head, J.W., 2000, Geologic map of the Lavinia Planitia (V-55) quadrangle, Venus: U.S. Geological Survey Geologic Investigations Series Map I-2684, scale 1:5,000,000 [in press].
- Janes, D.M., and Squyres, S.W., 1993, Radially fractured domes—A comparison of Venus and Earth: *Geophysical Research Letters*, v. 20, p. 2961–2964.
- Janes, D.M., Squyres, S.W., Bindschadler, D.L., Baer, G., Schubert, G., Sharpton, V.L., and Stofan, E.R., 1992, Geophysical models for the formation and evolution of coronae on Venus: *Journal of Geophysical Research*, v. 97, p. 16,055–16,067.
- Kiefer, W.S., and Hager, B.H., 1991, A mantle plume model for the equatorial highlands of Venus: *Journal of Geophysical Research*, v. 96, p. 20,947–20,966.
- Masursky, H., Eliason, E., Ford, P.G., McGill, G.E., Pettengill, G.H., Schaber, G.G., and Schubert, G., 1980, Pioneer Venus radar results—Geology from images and altimetry: *Journal of Geophysical Research*, v. 85, p. 8232–8260.
- Maxwell, T.A., El Baz, F., and Ward, S.H., 1975, Distribution, morphology, and origin of ridges and arches in Mare Serenitatis: *Geological Society of America Bulletin*, v. 86, p. 1273–1278.
- McGill, G.E., 1993, Wrinkle ridges, stress domains, and kinematics of venusian plains: *Geophysical Research Letters*, v. 20, p. 2407–2410.
- 1994a, Can the stratigraphic positions of impact craters constrain the temporal variability of venusian tectonic activity?: *Eos, Transactions of the American Geophysical Union, Supplement for 1994 Spring Meeting*, v. 75, p. 215.
- 1994b, Hotspot evolution and venusian tectonic style: *Journal of Geophysical Research*, v. 99, p. 23,149–23,161.
- McGovern, P.J., Jr., 1996, Studies of large volcanoes on the terrestrial planets—Implications for stress state, tectonics, structural evolution, and moat filling: Ph.D. Dissertation, Massachusetts Institute of Technology, Cambridge, Mass., 339 p.
- Muhleman, D.O., 1964, Radar scattering from Venus and the Moon: *Astronomical Journal*, v. 69, p. 34–41.
- Pavri, B., Head, J.W., Klose, K.B., and Wilson, L., 1992, Steep-sided domes on Venus—Characteristics, geologic setting, and eruption conditions from Magellan data: *Journal of Geophysical Research*, v. 97, p. 13,445–13,478.
- Phillips, R.J., and Malin, M.C., 1983, The interior of Venus and tectonic implications, in Hunten, D.M. and others, ed., *Venus: Tucson*, University of Arizona Press, p. 159–214.
- Plescia, J.B., and Golombek, M.P., 1986, Origin of planetary wrinkle ridges based on the study of terrestrial analogs: *Geological Society of America Bulletin*, v. 97, p. 1289–1299.
- Rosenberg, E., and McGill, G.E., 2001, Geologic map of the Pandrosos Dorsa quadrangle (V-5), Venus: U.S. Geological Survey Geologic Investigations Series Map I-2721, scale 1:5,000,000 [in press].
- Senske, D.A., Schaber, G.G., and Stofan, E.R., 1992, Regional topographic rises on Venus—Geology of western Eistla Regio and comparison to Beta Regio and Atla Regio: *Journal of Geophysical Research*, v. 97, p. 13,395–13,420.
- Solomon, S.C., Head, J.W., Kaula, W.M., McKenzie, D., Parsons, B., Phillips, R.J., Schubert, G., and Talwani, M., 1991, Venus tectonics—Initial analysis from Magellan: *Science*, v. 252, p. 297–312.
- Solomon, S.C., McGovern, P.J., Simons, M., and Head, J.W., 1994, Gravity anomalies over volcanoes on Venus—Implications for lithospheric thickness and volcano history, in Abstracts submitted to the Twenty-fifth Lunar and Planetary Science Conference, part 3, Houston, March 14–18, 1994: Houston, Lunar and Planetary Institute, p. 1317–1318.
- Solomon, S.C., Smrekar, S.E., Bindschadler, D.L., Grimm, R.E., Kaula, W.M., McGill, G.E., Phillips, R.J., Saunders, R.S., Schubert, G., Squyres, S.W., and Stofan, E.R., 1992, Venus tectonics—An overview of Magellan observations: *Journal of Geophysical Research*, v. 97, p. 13,199–13,255.
- Squyres, S.W., Janes, D.M., Baer, G., Bindschadler, D.L., Schubert, G., Sharpton, V.L., and Stofan, E.R., 1992a, The morphology and evolution of coronae on Venus: *Journal of Geophysical Research*, v. 97, p. 13,611–13,634.
- Squyres, S.W., Jankowski, D.G., Simons, M., Solomon, S.C., Hager, B.H., and McGill, G.E., 1992b, Plains tectonism on Venus—The deformation belts of Lavinia Planitia: *Journal of Geophysical Research*, v. 97, p. 13,579–13,599.
- Stofan, E.R., and Saunders, R.S., 1990, Geologic evidence of hotspot activity on Venus—Predictions for Magellan: *Geophysical Research Letters*, v. 17, p. 1377–1380.
- Stofan, E.R., Sharpton, V.L., Schubert, G., Baer, G., Bindschadler, D.L., Janes, D.M., and Squyres, S.W., 1992, Global distribution and characteristics of coronae and related features on Venus—Implications for origin and relation to mantle processes: *Journal of Geophysical Research*, v. 97, p. 13,347–13,378.
- Strom, R.G., Schaber, G.G., and Dawson, D.D., 1994, The global resurfacing of Venus: *Journal of Geophysical Research*, v. 99, p. 10,899–10,926.
- Sukhanov, A.L., Pronin, A.A., Burba, G.A., Nikishin, A.M., Kryuchkov, V.P., Basilevsky, A.T., Markov, M.S., Kuzmin, R.O., Bobina, N.N., Shashkina, V.P., Slyuta, E.N., and Chernaya, I.M., 1989, Geomorphologic/geologic map of part of the northern hemisphere of Venus: U.S. Geological Survey Miscellaneous Investigations Series Map I-2059, scale 1:15,000,000.
- Turcotte, D.L., 1995, How does Venus lose heat?: *Journal of Geophysical Research*, v. 100, p. 16,931–16,940.

**Table 1. Radar properties of map units.**

[Units are identified with symbols used on map and legend. Number below unit designation is sample station number. Lat/Long are coordinates of sampled area, and #pxls is number of non-zero pixels in that area. Incidence angle,  $i$ , in degrees, is angle between the SAR beam and the normal to a sphere where the beam intersects the surface;  $\sigma_o$  is normalized radar backscatter in decibels; rms is root mean square average of meter and larger scale slopes. Values of  $\sigma_o$  in parentheses are  $\pm$  one standard deviation about the mean; all other parameter values in parentheses represent the total ranges within sampled area. The two values of dielectric constant,  $\epsilon_s$  and  $\epsilon_r$ , represent probable extreme values for smooth and rough surfaces, respectively. Data with incidence angles of  $44^\circ$ – $46^\circ$  are from cycle 1 left-looking images; data with incidence angles of  $25^\circ$ – $26^\circ$  are from cycle 3 left-looking images. For most stations, sample areas from cycles 1 and 3 exactly coincide, and all values except radar backscatter are identical, and thus not repeated. All data are from C1\_MIDR's at 225 m/pxl]

Unit Station #	Lat/Long	#pxls	$i$	Radius, km	$\sigma_o$ , dB	rms slope, deg	Reflectivity	Emissivity	$\epsilon_s, \epsilon_r$
<b>Tessera Material</b>									
t 1	17.591–17.776N 12.786–13.001E	8712	45	6052.032 (6051.730,6052.212)	–11.705 (–19.348,–9.085)	3.42 (0.80,4.60)	.069 (.060,.085)	.858 (.846,.867)	2.9, 4.5
t 1	17.591–17.663N 12.784–13.001E	3465	26	6052.066 (6051.961,6052.164)	– 8.804 (–18.632, –6.026)	3.95 (3.80,4.40)	.063 (.060,.070)	.855 (.846,.859)	3.0, 4.7
t 2	5.885– 5.985N 17.830–17.934E	2352	46	6052.332 (6052.126,6052.413)	–10.023 (–18.268, –7.351)	4.26 (3.50,5.10)	.087 (.080,.105)	.864 (.861,.867)	2.8, 4.3
t 2		2340	25		– 8.830 (–18.729, –6.047)				
t 3	6.332– 6.351N 18.008–18.041E	160	46	6051.688 (6051.577,6051.798)	–10.332 (–12.841, –8.753)	4.75 (4.50,5.00)	.153 (.140,.165)	.832 (.830,.833)	3.3, 5.4
t 3			25		– 9.873 (–12.521, –8.240)				
<b>Plains Materials</b>									
ps 1	18.131–18.168N 12.829–12.880E	432	45	6051.515 (6051.481,6051.584)	–22.744 (–25.901,–20.935)	0.82 (0.70,1.00)	.164 (.100,.200)	.829 (.827,.831)	3.4, 5.5
ps 2	16.531–16.693N 16.039–16.178E	5082	46	6051.833 (6051.805,6051.900)	–20.197 (–21.402,–19.254)	1.51 (1.00,2.00)	.126 (.120,.130)	.810 (.807,.813)	3.7, 6.1
ps 2			26		–12.661 (–14.060,–11.605)				
ph 1	23.607–23.688N 26.615–26.752E	2340	44	6051.659 (6051.625–6051.746)	–15.785 (–16.803,–14.960)	1.87 (1.80,2.00)	.083 (.075,.090)	.880 (.875,.884)	2.7, 4.0
ph 2	24.548–24.652N 29.398–29.502E	2300	44	6051.006 (6050.999,6051.026)	–14.677 (–15.694,–13.853)	5.84 (4.50,7.70)	.082 (.075,.095)	.920 (.912,.927)	2.2, 3.0
ph 3	22.692–22.884N 30.100–30.345E	9919	44	6051.346 (6051.247,6051.448)	–16.192 (–17.386,–15.256)	2.99 (1.90,4.10)	.075 (.065,.085)	.899 (.886,.906)	2.4, 3.5
psl 1	22.977–23.692N 5.910– 6.400E	72118	44	6051.278 (6051.040,6051.403)	–16.630 (–18.955,–15.124)	1.82 (1.30,3.50)	.077 (.020,.105)	.849 (.838,.858)	3.1, 4.8
psl 2	20.943–21.556N 19.100–19.620E	65314	45	6051.165 (6051.029,6051.313)	–18.464 (–20.180,–17.237)	3.40 (2.50,4.30)	.106 (.090,.125)	.818 (.813,.822)	3.6, 5.9
pr <sub>c</sub> 1	10.069–10.148N –0.025– 0.064E	1558	46	6051.144 (6051.104,6051.171)	–12.835 (–14.001,–11.916)	1.92 (1.70,2.10)	.075 (.075,.075)	.838 (.837,.839)	3.2, 5.2
pr <sub>b</sub> 1	17.384–17.467N 10.093–10.146E	1000	45	6051.463 (6051.441,6051.491)	–18.737 (–19.836,–17.861)	2.50 (2.30,2.80)	.095 (.095,.095)	.839 (.837,.841)	3.2, 5.1
pr <sub>b</sub> 1			26		–13.598 (–14.895,–12.600)				
pr <sub>b</sub> 2	–0.204–0.075N 24.046–24.142E	2852	45	6050.912 (6050.877,6050.941)	–19.632 (–20.975,–18.607)	1.58 (1.20,1.90)	.103 (.095,.110)	.834 (.831,.837)	3.3, 5.3
pr <sub>b</sub> 2			25		–12.407 (–14.405,–11.043)				
pr <sub>b</sub> 4	3.569– 3.650N 9.100– 9.139E	741	46	6050.715 (6050.674,6050.744)	–17.748 (–19.089,–16.725)	3.12 (2.70,3.50)	.106 (.095,.115)	.837 (.836,.840)	3.2, 5.2

**Table 1. Radar properties of map units—Continued.**

Unit Station #	Lat/Long	#pxls	i	Radius, km	$\sigma_o$ , dB	rms slope, deg	Reflectivity	Emissivity	$\epsilon_s, \epsilon_f$
<b>Plains Materials—continued</b>									
pr <sub>b</sub> <sub>4</sub>			25		-11.082 (-12.841, -9.834)				
pr <sub>b</sub> <sub>5</sub>	12.289–12.329N 6.357– 6.412E	520	46	6051.200 (6051.182,6051.210)	-14.935 (-16.904,-13.585)	2.07 (2.00,2.10)	.102 (.100,.105)	.845 (.844,.846)	3.1, 4.9
pr <sub>b</sub> <sub>5</sub>			26		-10.016 (-11.612, -8.852)				
pr <sub>a</sub> <sub>1</sub>	2.546– 2.620N 4.559– 4.622E	1080	46	6050.829 (6050.822,6050.839)	-11.805 (-13.062,-10.832)	1.63 (1.50,1.70)	.112 (.110,.115)	.820 (.820,.821)	3.5, 5.8
pr <sub>a</sub> <sub>2</sub>	4.155– 4.233N 1.903– 1.987E	1520	46	6051.165 (6051.069,6051.190)	-14.353 (-15.668,-13.345)	2.03 (1.90,2.30)	.091 (.090,.095)	.838 (.836,.840)	3.2, 5.2
pr <sub>a</sub> <sub>3</sub>	12.078–12.170N 1.328– 1.348E	396	46	6052.037 (6051.975,6052.099)	-16.096 (-17.473,-15.051)	2.07 (2.00,2.20)	.088 (.075,.100)	.823 (.822,.824)	3.4, 5.7
pt <sub>1</sub>	15.401–15.482N 18.467–18.529E	1092	46	6051.980 (6051.905,6052.059)	-13.837 (-16.207,-12.312)	4.22 (3.50,5.20)	.091 (.080,.100)	.825 (.822,.828)	3.4, 5.6
pt <sub>1</sub>			26		-9.390 (-12.118, -7.728)				
pl <sub>1</sub>	23.258–23.346N 13.118–13.230E	2100	44	6051.051 (6051.048,6051.058)	-12.327 (-14.486,-10.891)	1.53 (1.10,1.90)	.088 (.085,.095)	.844 (.837,.848)	3.2, 5.0
pl <sub>2</sub>	17.023–17.078N 9.290– 9.312E	297	45	6051.480 (6051.471,6051.489)	-8.401 (-12.077, -6.439)	3.10 (2.80,3.40)	.107 (.100,.115)	.863 (.863,.864)	2.8, 4.4
pl <sub>2</sub>			26		-7.527 (-11.645, -5.453)				
pl <sub>3</sub>	19.549–19.662N 5.132– 5.169E	864	45	6051.711 (6051.652,6051.779)	-7.950 (-14.192, -5.489)	4.03 (3.90,4.20)	.079 (.075,.085)	.853 (.852,.855)	3.0, 4.7
<b>Corona Materials</b>									
fcN <sub>1</sub>	13.536–13.606N 9.261– 9.314E	1020	46	6051.464 (6051.418,6051.498)	-12.738 (-13.870,-11.840)	2.12 (2.10,2.20)	.130 (.120,.140)	.827 (.825,.830)	3.4, 5.5
fcN <sub>1</sub>			26		- 8.512 (-10.278, -7.259)				
fcN <sub>2</sub>	16.682–16.718N 10.045–10.087E	360	46	6051.612 (6051.587,6051.648)	-18.398 (-19.730,-17.380)	2.25 (2.10,2.40)	.104 (.100,.105)	.831 (.830,.831)	3.3, 5.4
fcN <sub>2</sub>			26		-11.822 (-13.487,-10.621)				
fcN <sub>3</sub>	16.933–17.067N 12.397–12.512E	3456	45	6052.068 (6051.967,6052.184)	-11.636 (-13.234,-10.470)	2.99 (2.40,4.00)	.081 (.025,.160)	.822 (.820,.823)	3.5, 5.7
fcN <sub>3</sub>			26		- 8.225 (-9.867, -7.037)				
fcB <sub>1</sub>	5.925– 6.025N 20.153–20.227E	1680	46	6051.247 (6051.174,6051.285)	-18.201 (-19.464,-17.225)	3.65 (3.30,4.00)	.085 (.085,.085)	.862 (.860,.864)	2.8, 4.4
fcB <sub>1</sub>			25		-11.656 (-13.291,-10.471)				
fcB <sub>2</sub>	5.819– 5.881N 20.228–20.303E	1080	46	6051.089 (6050.973,6051.138)	-18.476 (-19.866,-17.424)	4.07 (3.90,4.20)	.090 (.090,.090)	.859 (.857,.860)	2.9, 4.5
fcB <sub>2</sub>			25		-12.527 (-13.927,-11.470)				
fca <sub>1</sub>	14.009–14.096N 7.016– 7.104E	1722	46	6051.543 (6051.470,6051.598)	-12.939 (-14.074,-12.040)	2.06 (1.60,2.40)	.104 (.095,.115)	.847 (.844,.850)	3.1, 4.9
fca <sub>1</sub>			26		-8.066 (-9.402, -7.045)				

**Table 1. Radar properties of map units—Continued.**

Unit Station #	Lat/Long	#pxls	<i>i</i>	Radius, km	$\sigma_0$ , dB	rms slope, deg	Reflectivity	Emissivity	$\epsilon_s$ , $\epsilon_r$
<b>Miscellaneous Dome and Flow Materials</b>									
fh 1	2.518–2.537N 27.369–27.431E	300	46	6051.125 (6051.113,6051.137)	–10.987 (–15.626, –8.795)	3.90 (3.70,4.10)	.105 (.100,.110)	.860 (.858,.862)	2.9, 4.5
fs 1	21.047–21.073N 15.639–15.672E	195	45	6050.884 (6050.883,6050.885)	–14.879 (–16.321,–13.798)	3.02 (2.90,3.20)	.137 (.135,.140)	.811 (.811,.811)	3.8, 6.1
fs 2	20.817–20.849N 15.396,15.406E	80	45	6050.977 (6050.970,6050.985)	–9.977 (–11.294, –8.968)	3.00 (2.80,3.30)	.119 (.110,.125)	.813 (.813,.813)	3.7, 6.1
fs 3	3.993– 4.016N 9.312– 9.372E	348	46	6050.542 (6050.541,6050.544)	–13.378 (–14.452,–12.518)	4.58 (4.30,4.90)	.101 (.100,.105)	.844 (.842,.846)	3.1, 5.0
fs 3			25		–8.635 (–10.032, –7.580)				
f 1	20.356–20.394N 7.977– 8.018E	361	45	6051.022 (6051.007,6051.031)	–8.887 ( –9.948, –8.035)	2.05 (1.70,2.50)	.094 (.090,.100)	.849 (.848,.851)	3.1, 4.8
f 2	21.418–21.507N 10.893–10.958E	1290	45	6050.780 (6050.758,6050.796)	–18.833 (–20.261,–17.761)	1.52 (1.30,1.70)	.104 (.100,.105)	.829 (.827,.831)	3.4, 5.5
dC 1	12.172–12.227N 7.463– 7.503E	513	46	6052.195 (6052.179–6052.222)	–15.018 (–16.172, –14.107)	2.48 (2.00,3.30)	.083 (.075,.095)	.851 (.846,.854)	3.0, 4.8
dC 1			26		–11.540 (–12.976, –10.463)				
dO 1	4.246– 4.284N 19.283–19.321E	361	46	6050.970 (6050.833–6051.140)	–17.133 (–18.316, –16.204)	3.95 (3.60,4.30)	.097 (.080,.120)	.855 (.851,.859)	2.9, 4.6
dO 1			25		–11.397 (–13.244, –10.105)				
<b>Materials of Volcanic Constructs</b>									
hA 1	11.546–11.640N 13.957–14.047E	1935	46	6053.428 (6053.387,6053.461)	–8.269 ( –9.549, –7.281)	3.47 (2.90,4.30)	.112 (.105,.120)	.833 (.828,.838)	3.3, 5.3
hA 1	11.546–11.640N 13.957–14.011E	1170	26		–6.775 ( –8.306, –5.645)				
hA 2	10.499–10.580N 14.088–14.173E	1599	46	6053.531 (6053.480,6053.598)	–11.961 (–13.440,–10.859)	4.30 (3.40,5.40)	.126 (.110,.130)	.794 (.778,.805)	3.9, 6.8
hA 2	10.499–10.580N 14.121–14.173E	975	26		–8.773 (–10.205, –7.698)				
mA 1	11.365–11.397N 14.205–14.237E	256	46	6052.983 (6052.958,6053.019)	–18.595 (–20.063,–17.501)	3.60 (3.40,3.90)	.150 (.150,.150)	.808 (.805,.811)	3.7, 6.2
mA 1			26		–12.045 (–13.128,–11.178)				
fhA 1	9.848– 9.909N 13.536–13.639E	1470	46	6052.524 (6051.860,6052.719)	–15.169 (–16.398,–14.213)	6.39 (5.60,7.10)	.068 (.055,.080)	.910 (.903,.915)	2.2, 3.1
fhA 1	9.848– 9.909N 13.563–13.639E	1080	26		–10.286 (–12.116, –9.002)				
fA 1	11.216–11.269N 11.884–11.925E	520	46	6051.806 (6051.804,6051.809)	–21.232 (–22.508,–20.247)	2.02 (1.90,2.10)	.141 (.140,.145)	.822 (.822,.822)	3.4, 5.7
fA 1			26		–13.020 (–14.576,–11.877)				
fA 2	11.078–11.123N 11.805–11.845E	440	46	6051.775 (6051.765,6051.785)	–16.151 (–17.655,–15.036)	2.93 (2.30,3.60)	.142 (.135,.150)	.822 (.822,.823)	3.4, 5.7
fA 3	10.442–10.493N 12.923–12.983E	725	46	6052.387 (6052.297,6052.474)	–12.125 (–13.596,–11.028)	4.25 (3.60,5.10)	.150 (.135,.175)	.826 (.823,.828)	3.4, 5.6

**Table 1. Radar properties of map units—Continued.**

Unit Station #	Lat/Long	#pxls	<i>i</i>	Radius, km	$\sigma_0$ , dB	rms slope, deg	Reflectivity	Emissivity	$\epsilon_s$ , $\epsilon_r$
<b>Materials of Volcanic Constructs—continued</b>									
fA 3			26		-8.437 (-10.571, -7.012)				
fA 4	12.402–12.455N 12.173–12.234E	754	46	6051.869 (6051.856,6051.887)	-23.119 (-24.233,-22.234)	1.33 (1.20,1.50)	.150 (.140,.165)	.805 (.802,.806)	3.8, 6.3
hl 1	15.750–15.971N 15.085–15.555E	22260	46	6052.047 (6051.725,6052.508)	-9.031 (-10.431, -7.974)	3.98 (2.60,5.90)	.095 (.060,.115)	.878 (.864,.894)	2.6, 4.0
hl 1			26		-6.733 (-8.734, -5.368)				
hl 2	15.807–16.012N 14.610–14.870E	11349	46	6051.999 (6051.720,6052.354)	-10.003 (-11.508,-8.888)	3.44 (2.20,4.70)	.093 (.075,.105)	.875 (.858,.895)	2.7, 4.1
hl 2			26		-7.492 (-9.288, -6.225)				
hl 3	15.126–15.292N 14.280–14.467E	6715	46	6052.565 (6052.367,6052.709)	-8.599 (-9.890, -7.606)	5.62 (3.70,7.50)	.127 (.100,.160)	.874 (.871,.877)	2.7, 4.1
hl 3		5324	26		-6.996 (-9.548, -5.399)				
ml 1	14.634–14.671N 15.483–15.518E	306	46	6052.522 (6052.513,6052.532)	-16.448 (-18.516,-15.053)	5.25 (4.90,5.60)	.123 (.120,.125)	.847 (.845,.850)	3.1, 4.9
ml 1			26		-10.585 (-13.469, -8.866)				
ml 2	14.883–14.903N 15.321–15.338E	90	46	6052.505 (6052.443,6052.568)	-20.162 (-21.463,-19.162)	4.40 (3.90,4.90)	.115 (.105,.125)	.839 (.833,.846)	3.2, 5.1
ml 2			26		-12.987 (-14.178,-12.053)				
fhl 1	14.485–14.513N 14.464–14.532E	448	46	6053.445 (6053.381,6053.524)	-9.672 (-11.345, -8.468)	6.67 (6.10,7.50)	.148 (.135,.160)	.809 (.802,.814)	3.7, 6.2
fhl 1			26		-6.825 (-9.114, -5.333)				
fl 1	13.983–14.073N 13.467–13.548E	1677	46	6052.033 (6051.994,6052.059)	-13.689 (-15.010,-12.677)	3.25 (2.90,4.00)	.145 (.140,.150)	.817 (.812,.822)	3.5, 5.9
fl 1			26		-9.490 (-11.491, -8.125)				
fl 2	13.926–14.000N 13.329–13.418E	1512	46	6052.048 (6052.027,6052.074)	-17.629 (-18.940,-16.624)	2.98 (2.60,3.40)	.119 (.115,.125)	.819 (.816,.821)	3.5, 5.8
fl 2			26		-11.755 (-13.363,-10.584)				
fl 3	12.632–12.661N 16.874–16.948E	525	46	6052.217 (6052.169,6052.259)	-16.165 (-17.349,-15.235)	3.25 (3.10,3.40)	.100 (.095,.105)	.813 (.811,.816)	3.6, 6.0
fl 3			26		-11.127 (-12.574,-10.043)				
fpK 1	8.779– 8.805N 29.910–29.932E	143	46	6053.063 (6053.017,6053.110)	-20.306 (-21.819,-19.186)	3.10 (2.90,3.30)	.090 (.090,.090)	.802 (.801,.803)	3.8,6.4
fpK 2	8.745– 8.779N 30.151–30.188E	306	46	6052.365 (6052.357,6052.388)	-14.660 (-16.161,-13.547)	3.08 (2.80,3.50)	.110 (.110,.110)	.800 (.798,.802)	3.8, 6.5
fpK 1	7.445– 7.504N 29.190–29.263E	1015	46	6051.467 (6051.426,6051.490)	-16.702 (-18.320,-15.525)	1.75 (1.40,2.10)	.102 (.080,.125)	.826 (.822,.837)	3.4, 5.6
fpK 2	7.453– 7.504N 29.895–29.946E	625	46	6051.332 (6051.307,6051.346)	-11.869 (-13.201,-10.851)	3.20 (2.50,3.70)	.082 (.080,.085)	.893 (.886,.899)	2.4, 3.5

**Table 1. Radar properties of map units—Continued.**

Unit Station #	Lat/Long	#pxls	<i>i</i>	Radius, km	$\sigma_o$ , dB	rms slope, deg	Reflectivity	Emissivity	$\epsilon_s$ , $\epsilon_r$
<b>Materials of Volcanic Constructs—continued</b>									
fG 1	23.248–23.309N 1.256– 1.341E	1080	44	6052.763 (6052.737,6052.829)	-13.374 (-15.257,-12.066)	4.32 (3.70,5.30)	.077 (.070,.085)	.853 (.851,.856)	3.1, 4.7
fG 1			25		-8.463 (-10.164, -7.244)				
fG 2	25.659–25.702N 0.435– 0.502N	588	44	6052.538 (6052.529,6052.551)	-16.795 (-18.595,-15.527)	2.03 (1.30,2.70)	.069 (.055,.080)	.860 (.857,.863)	3.0, 4.6
fG 2			25		-11.170 (-12.609,-10.092)				
<b>Annia Faustina ejecta (2 stations)</b>									
# 1	22.167–22.224N 4.770– 4.843E	896	45	6051.791 (6051.763,6051.816)	-11.341 (-14.552, -9.516)	2.10 (1.90,2.30)	.075 (.075,.075)	.833 (.826,.839)	3.4, 5.4
# 2	22.146–22.218N 4.519– 4.572E	805	45	6051.849 (6051.831,6061.875)	-11.723 (-15.377, -9.768)	0.87 (0.80,0.90)	.133 (.105,.210)	.814 (.808,.819)	3.7, 6.0
# 2			25		-5.727 (-9.357, -3.778)				
<b>Callas ejecta (#1), central peak (#2), and floor (#3)</b>									
# 1	2.399– 2.580N 26.810–26.904E	3870	46	6050.967 (6050.800,6051.198)	-10.607 (-15.662, -8.334)	2.21 (1.60,2.90)	.089 (.085,.095)	.856 (.851,.861)	2.9, 4.6
# 2	2.420– 2.443N 26.985–27.025E	240	46	6050.311 (6050.302,6050.319)	-7.129 (-15.174, -4.474)	0.80 (0.50,1.10)	.122 (.110,.135)	.864 (.863,.864)	2.8, 4.4
# 3	2.414– 2.445N 26.919–26.957E	304	46	6050.604 (6050.304,6050.927)	-17.816 (-20.019,-16.361)	1.80 (1.10,2.50)	.111 (.090,.150)	.862 (.861,.863)	2.8, 4.4
<b>Piaf ejecta (# 1), floor (# 2), and flow (# 3)</b>									
# 1	.879– .902N 5.556– 5.603E	276	45	6050.941 (6050.926,6050.957)	-9.591 (-11.436, -8.300)	2.75 (2.60,2.90)	.093 (.090,.095)	.868 (.868,.868)	2.8, 4.3
# 2	.890– .911N 5.296– 5.347E	275	45	6050.808 (6051.791,6050.825)	-14.955 (-16.207,-13.983)	2.25 (2.20,2.30)	.087 (.085,.090)	.862 (.862,.863)	2.9, 4.4
# 3	1.352– 1.388N 5.300– 5.341E	360	45	6050.702 (6050.693,6050.708)	-12.371 (-13.602,-11.412)	2.17 (2.10,2.30)	.097 (.090,.105)	.846 (.844,.849)	3.1, 4.9